Chinese Chemical Letters 33 (2022) 271–275

Contents lists available at ScienceDirect

Chinese Chemical Letters

journal homepage: www.elsevier.com/locate/cclet

S/Se-embedded acenaphthylene-imide-containing polycyclic heteroaromatic hydrocarbon

Zhichao Wang[a], Qianli Ma[a], Xuan Huang[a], Tian Zhang[a], Jiawei Shao[b], Xinglin Zhang[a], Qian Shen[a,*], Xiaochen Wang[c,*], Jinjun Shao[a,*]

[a] Key Laboratory of Flexible Electronics (KLOFE) & Institute of Advanced Materials (IAM), Nanjing Tech University (NanjingTech), Nanjing 211800, China
[b] Department of Chemistry, National University of Singapore, Singapore 117543, Singapore
[c] School of Materials Science & Engineering, Shaanxi Normal University, Xi'an 710119, China

ARTICLE INFO

Article history:
Received 28 April 2021
Revised 23 June 2021
Accepted 25 June 2021
Available online 2 July 2021

Keywords:
Acenaphthylene-imide
Polycyclic aromatic hydrocarbons
Protonation
Selenium
Condensation

ABSTRACT

Acenapththylene-imide (AnI), similar to naphthalene diimide (NDI), is an outstanding building block for organic functional materials and has gained a lot of research attention. Herein, Sulphur and Selenium-embedded AnI-containing polycyclic aromatic hydrocarbon molecules, AnI-SQ and AnI-SeQ, with [1,2,5]thiadiazolo[3,4-*g*]quinoxaline (SQ) and [1,2,5]selenadiazolo[3,4-*g*]quinoxaline (SeQ) are designed and synthesized with low-lying LUMO energy levels. The absorption and emission of AnI-SQ and AnI-SeQ displayed a bathochromic shift upon protonation of the C = N bond. Besides, theoretical calculation indicates remarkable rigid planar backbones for both AnI-SQ and AnI-SeQ. Through self-assembly with polymeric Pluronic® F-127, corresponding hydrophilic nanoparticles (NPs) were prepared with low cytotoxicity. And AnI-SQ NPs could be applied for *in vitro* two-photon fluorescence imaging.

Polycyclic aromatic hydrocarbons (PAHs), especially the highly planar and linearly fused oligoacenes, have gained increasing research attention from chemists, physicists, and material scientists [1]. Owing to the unique extended π-conjugated structures, the optoelectronic and electrochemical properties of PAHs can be easily tuned to meet people's demands [2]. Moreover, it was demonstrated that they possessed many applications in bioelectronic and organic electronic devices [3-5]. Through the incorporation of heteroatoms into PAH, the polycyclic heteroaromatic hydrocarbons (PHAHs) can be obtained with various interesting features [6,7], rendering them one of the essential organic semiconducting materials for organic field-effect transistors (OFETs), organic light-emitting diodes (OLEDs) and organic solar cells [8,9]; In addition, PHAHs have been widely applied for bio-imaging and cancer therapy with superior performance, through proper functionalization to endow excellent biosafety and low systemic toxicity [10-18].

Acenaphthylene-imide (AnI), with a naphthalene moiety and an imide group, was an essential building block for PHAHs. Similar to naphthalene diimide (NDI), AnI possesses many advantages, such as low-lying LUMO energy levels *via* modification with the electron-deficient group and desirable solubility and processability through inserting alkyl chain into the imide group [19-22]. Besides, different from NDI, AnI could be easily fused at the longitudinal direction to extend the π-conjugation without sacrificing the imide group. There are many PHAHs based on AnI have been prepared *via* fusion of various group (such as thiophene) or electron-deficient moieties onto AnI [23]. Jenekhe *et al.* reported a family of AnI derived PHAHs *via* longitudinal π-extension to fuse with 2,3,5,6-tetraaminoterephthalonitrile or 3,6-di(thiophen-2-yl)benzene-1,2,4,5-tetraamine, which show low-lying LUMO energy levels and excellent device performance [24-26]. In addition, we also reported a series of AnI-based PHAHs with LUMO energy levels lowered to −4.03 eV, and some were applied as non-fullerene electron-transporting layer for perovskite solar cells with a good power conversion efficiency [27].

Moreover, [1,2,5]thiadiazolo[3,4-*g*]quinoxaline (SQ) has been widely used as the strong accepter unit to construct the PHAHs with low bandgap [28,29]. Many near-infrared (NIR) molecules with SQ units were exploited for bioimaging or organic electronic devices [30]. Wang *et al.* prepared a series of SQ-containing narrow-bandgap compounds showing the maximum NIR absorption peak at 1177 nm [31]. Additionally, Selenium (Se) comes from the chalcogen family and displays similar photophysical properties as sulfur (S) [32]. However, Se atom in [1,2,5]selenadiazolo[3,4-*g*]quinoxaline (SeQ) exhibits relatively stronger Se-Se intermolecu-

* Corresponding authors.
E-mail addresses: iamqshen@njtech.edu.cn (Q. Shen), wangxc@snnu.edu.cn (X. Wang), iamjjshao@njtech.edu.cn (J. Shao).

https://doi.org/10.1016/j.cclet.2021.06.072
1001-8417/

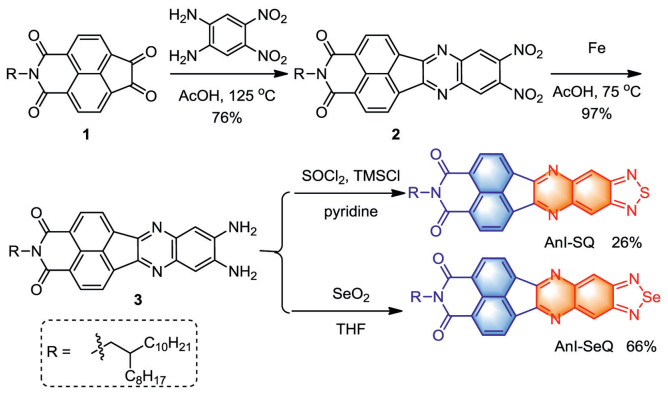

Scheme 1. Synthetic route for AnI-SQ and AnI-SeQ.

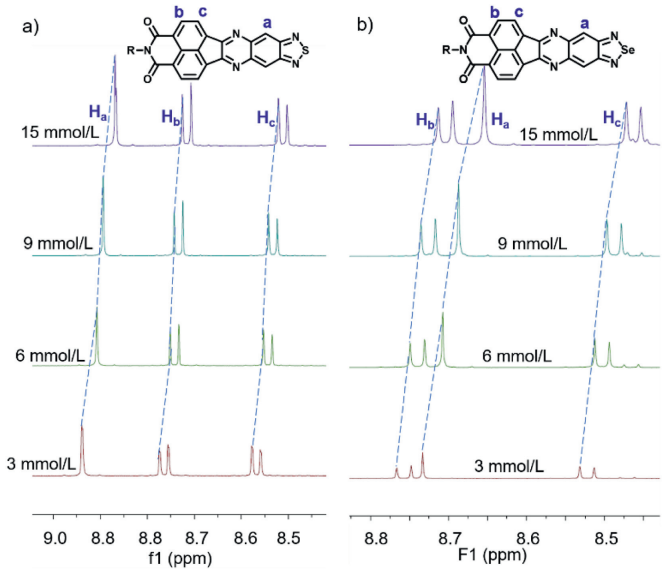

Fig. 1. Partial ^{1}H NMR spectra of AnI-SQ (a) and AnI-SeQ (b) at different concentrations in $CDCl_3$ at 298 K.

lar interactions, which lead to a significant difference between SeQ and SQ in the molecular packing mode and optoelectronic properties. Therefore, the SeQ unit has attracted increasing attention recently, and a large number of SeQ-containing molecules have been exploited for various applications.

Herein, two PHAH molecules AnI-SQ and AnI-SeQ were prepared through fusing AnI moiety with SQ and SeQ units, respectively (Scheme 1). Both AnI-SQ and AnI-SeQ with low-lying LUMO energy levels show C_2 symmetry and rigid planar structures [33]. Besides, *via* enveloping hydrophobic AnI-XQ (X = S, Se) with amphiphilic Pluronic® F-127, AnI-XQ nanoparticles (NPs) can be obtained with low cytotoxicity and biosafety. And AnI-SQ NPs can be further applied for two-photon fluorescence imaging in living cells.

As shown in Scheme 1, the condensation reaction between **1** [27] and 4,5-dinitrobenzene-1,2-diamine [34] was carried out in the acetic acid to give **2** in good yield, which was subsequently reduced with iron powder in acetic acid to obtain air-stable diamine **3** with 97% yield. Compound **3** was treated with $SOCl_2$ in pyridine and THF to furnish AnI-SQ, and AnI-SeQ was prepared by treating **3** and SeO_2 in THF. Nuclear magnetic resonance (NMR) spectroscopy (^{1}H NMR, ^{13}C NMR) and MALDI-TOF mass spectrometry was applied to identify the chemical structures and purity of AnI-SQ and AnI-SeQ (Supporting information).

It was noticeable in Fig. 1 that the concentration-dependent ^{1}H NMR spectra of AnI-SQ and AnI-SeQ in $CDCl_3$ solution could be observed. For AnI-SQ, as the concentration increased from 3 mmol/L to 15 mmol/L in $CDCl_3$, the resonance signals of the three aromatic peaks all shifted to high-field with chemical shift change ($\Delta\delta$) of 0.07 ppm for H_a, 0.04 ppm for H_b, and 0.06 ppm for H_c (H_a moved from 8.94 to 8.87 ppm, H_b moved from 8.75 to 8.71 ppm and H_c moved from 8.58ppm to 8.52 ppm). In comparison to AnI-SQ, owing to the stronger Se···Se intermolecular interactions, $\Delta\delta$ of AnI-SeQ was larger than AnI-SQ when the concentration increased. As shown in Fig. 1b, all aromatic proton signals (a/b/c) showed an up-field shift with respective $\Delta\delta$ of 0.16, 0.09, and 0.07 ppm (H_a moved from 8.75ppm to 8.66 ppm, H_b moved from 8.87ppm to 8.71 ppm, and H_c moved from 8.55ppm to 8.48 ppm) when the concentration increased from 3 mmol/L to 15 mmol/L. Such an up-field shift phenomenon for the aromatic protons in AnI-SQ and AnI-SeQ could be explained by the fact that it is the influence of the ring current from the neighboring molecule, and AnI-SeQ demonstrates a higher tendency than AnI-SQ to self-associate through strong intermolecular interactions [35].

The UV–vis absorbance and photoluminescence (PL) of AnI-SQ and AnI-SeQ in CH_2Cl_2 were recorded for investigation (Table 1, Fig. S1 in Supporting information). The absorption spectra of AnI-SQ and AnI-SeQ are similar, with two well-resolved absorption bands peaked at 355/371 nm and 372/387 nm, respectively. The absorption peak at 355 nm for AnI-SQ and 372 nm for AnI-SeQ were led from the π-π^* transition; while the corresponding absorption band peaked at 371 and 387 nm may result from the intramolecular charge transfer (ICT) [36]. Besides, the optical energy gap (E_g^{opt}) was calculated to be 2.83 eV for AnI-SQ and 2.95 eV for AnI-SeQ, respectively.

It is interesting to note that there are three fluorescence peaks for both AnI-SQ and AnI-SeQ in CH_2Cl_2. For AnI-SQ, two fluorescence bands were observed with peaks at 405 nm and 428 nm, and one broad fluorescence band was found to cover from 450 nm to 650 nm (Fig. S1a). While AnI-SeQ displayed two sharp fluorescence peaks, which are found to be the same as that of AnI-SQ, and one shoulder fluorescence band covering from 450 nm to 550 nm (Fig. S1b). Thus, and the respective Stokes shift was calculated to be 6462 cm^{-1} and 2475 cm^{-1} for AnI-SQ and AnI-SeQ, respectively. Furthermore, the quantum yields (ϕ) of AnI-SQ and AnI-SeQ were investigated, and it is calculated to be 1.1% and 0.5% for AnI-SQ and AnI-SeQ, respectively, by taking quinine sulfate (0.1 mol/L H_2SO_4, $\phi = 0.54$) as a reference [37]. The lower fluorescence quantum yield of AnI-SeQ is probably due to the fact that Se is a heavy atom, which will increase the probability of intersystem crossing. The fluorescence lifetimes of AnI-SQ and AnI-SeQ in CH_2Cl_2 were measured to be 1.37 ns and 1.38 ns, respectively, through time-correlated single photon counting (TCSPC) method (Fig. S1c). Therefore, the radiative decay constant (k_r) and non-radiative decay constant (k_{nr}) for AnI-SQ was determined to be 8.03×10^6 s^{-1} and 7.22×10^8 s^{-1}, respectively. Nevertheless, the k_r was 3.62×10^6 s^{-1} only for AnI-SeQ, the k_{nr} for AnI-SQ and AnI-SeQ was almost the same.

Additionally, both AnI-SQ and AnI-SeQ showed excellent photostability in toluene (Fig. S2 in Supporting information). Under Xe lamp irradiation, the commercial dye Fluorescein exhibited apparent decomposition, the maximum absorption peak of fluorescein diminished within 50 min, while there were almost no decompositions under the same condition for both AnI-SQ and AnI-SeQ under the same condition.

Also, with the embedment of imine moieties, AnI-XQ demonstrates an acid stimulus-responsive behavior due to the protonation of the C=N units [38]. With the addition of trifluoroacetic acid (TFA) into AnI-SQ solution (from 180 equiv. to 1080 equiv.), the absorption peaks had a slight red-shift; after neutralization by adding triethylamine (TEA), the adsorption profiles

Table 1
Photophysical properties for AnI-SQ and AnI-SeQ.

Compound	λ_{abs}^{max} (nm)	λ_{emi}^{max} (nm)	Stokes Shift (cm^{-1})[a]	λ_{onset} (nm)	τ_s (ns)[b]	$k_r(s^{-1})$	$k_{nr}(s^{-1})$	E_g^{opt} (eV)[c]	E_{red}^{onset} (V)	HOMO (eV)		LUMO (eV)		E_g (eV)[e]
										CV[d]	Calc[e]	CV[d]	Calc[e]	
AnI-SQ	371	488	6462	438	1.37	8.03×10^6	7.22×10^8	2.83	−1.15	−6.48	−6.33	−3.65	−3.32	3.01
AnI-SeQ	387	428	2475	420	1.38	3.62×10^6	7.20×10^8	2.95	−1.35	−6.40	−6.21	−3.45	−3.38	2.83

[a] Stokes shift = $1/\lambda_{abs}^{max}$ - $1/\lambda_{emi}^{max}$.
[b] Fluorescence lifetime.
[c] E_g^{opt} was measured from the lowest-energy absorption edge in CH_2Cl_2.
[d] HOMO/LUMO energy levels were calculated from the CV results.
[e] Calculated by the B3LYP/6–31G(d,p) basis set.

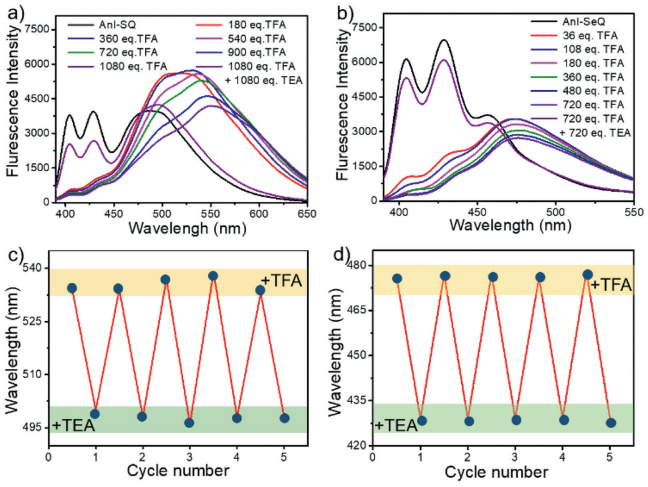

Fig. 2. Fluorescence emission spectra of AnI-SQ (a) and AnI-SeQ (b) in CH_2Cl_2 with subsequent addition of TFA. Maximum emission intensity changes by adding TFA and TEA alternately into AnI-SQ (c) and AnI-SeQ solution (d).

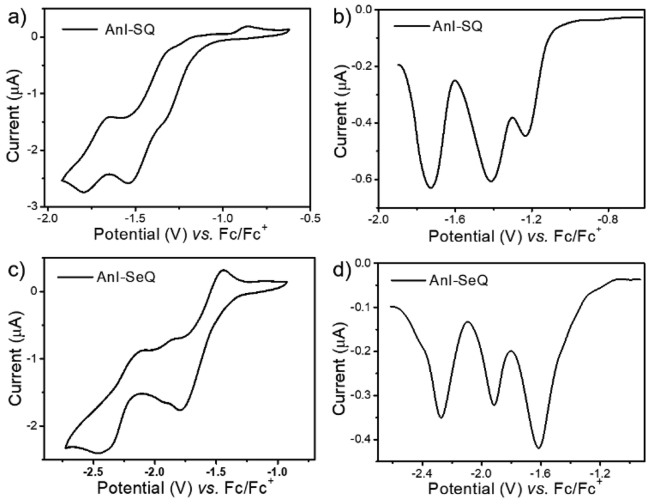

Fig. 3. Cyclic voltammetry and differential pulse voltammetry curves for AnI-SQ (a, b) and AnI-SeQ (c, d) in dry dichloromethane.

could be recovered (Fig. S3 in Supporting information), indicating reversible protonation-deprotonation progress of AnI-SQ. Furthermore, tremendous changes of the fluorescence spectra could be observed for AnI-SQ, the emissions at ~404 nm and ~428 nm were weakened with the gradual addition of TFA. And the maximum emission peak red-shifted obviously, and the red-shift was up to ~373 nm with 210 mmol/L addition of TFA. Also, the solution color was changed from green to yellow under 365 nm ultraviolet lamp (Fig. S4 in Supporting information). Subsequent neutralization by adding TEA, such changes for the fluorescences spectra and solution color could be recovered. Besides, AnI-SeQ also showed a similar phenomenon, the absorption peaks had a slight red-shift when adding TFA into AnI-SeQ solution (from 36 equiv. to 720 equiv.), after neutralizing by TEA, the original absorption spectrum could be observed, and the color of the solution was recovered (Fig. S4). Moreover, once TFA was added, the intensity of emission peaks at ~405/428 nm was diminished, and the maximum emission peak at ~475 nm even appeared. Nevertheless, the fluorescence spectrum could also be recovered to the original after the addition of TEA. Additionally, with the alternate addition of TFA and TEA into AnI-SQ or AnI-SeQ solution for five cycles, the peak of the maximum emission band presented corresponding changes (Fig. 2b), as indicated the outstanding stability towards the acid stimulus-response of AnI-SQ and AnI-SeQ with reversible and sensitive acid-responsive characteristics. AnI-SQ and AnI-SeQ exhibit great potential for the application in reusable-acid sensors in the future.

To improve the hydrophilicity, AnI-SQ NPs and AnI-SeQ NPs were prepared *via* self-assembly by employing amphiphilic copolymer Pluronic®F-127 as the matrix. Both NPs exhibited excellent water solubility and photostability, and showed yellow-green and yellow color for AnI-SQ NPs and AnI-SeQ NPs, respectively. Dynamic light scattering (DLS) results indicated that the diameter of AnI-SQ NPs and AnI-SeQ NPs was around 107 nm and 132 nm, respectively (Fig. S5 in Supporting information). The UV–vis absorbance and photoluminescence of AnI-SQ NPs and AnI-SeQ NPs were measured in water (Fig. S5), the respective maximum absorption/fluorescence peaks were 317/545 nm and 330/581 nm, respectively; and the Stokes shift was calculated to be 228 nm for AnI-SQ NPs, and 261 nm for AnI-SeQ NPs. The quantum yields of AnI-SQ NPs and AnI-SeQ NPs were measured to be 1.4% and 0.02%, respectively. Besides, owing to the intermolecular interactions in the aggregates after the formation of NPs, the absorption spectra presented a respective blue shift of 54 nm and 57 nm for AnI-SQ NPs and AnI-SeQ NPs, respectively. Additionally, both AnI-SQ NPs and AnI-SeQ NPs exhibited excellent photostability in water; the maximum absorption peaks of AnI-SQ NPs and AnI-SeQ NPs displayed almost no decrease within 40 min under Xe lamp irradiation (Fig. S6 in Supporting information).

The electrochemical properties of AnI-SQ and AnI-SeQ were investigated by cyclic voltammetry (CV) and differential pulse voltammetry (DPV) in dry dichloromethane. As illustrated in Figs. 3a and b, three quasi-reversible reduction waves could be seen for AnI-SQ, with the onset reduction potential E_{red}^{onset} at −1.15 V, and the half-wave potential $E_{red}^{1/2}$ at −1.73 V, −1.42 V, and −1.23 V. Similarly, AnI-SeQ also displayed three *quasi*-reversible reduction waves (Figs. 3c and d), exhibiting E_{red}^{onset} at −1.35 V with $E_{red}^{1/2}$ at −2.27 V, −1.91 V and −1.61 V. Additionally, none oxidation peaks were found for both AnI-SQ and AnI-SeQ. Moreover, the HOMO/LUMO energy levels of AnI-SQ and AnI-SeQ are calculated to be −6.48/−3.65 eV and −6.40/−3.45 eV, respectively. The LUMO

energy level for AnI-SeQ was 0.20 eV lower than AnI-SQ; this is probably due to the exceptional electronegativity of the hypervalent Se.

To further study the molecular electronic/geometric structures, the electron density distribution and the molecular architecture fundamentals of AnI-SQ and AnI-SeQ were theoretically investigated through time-dependent density functional theory (TD-DFT) calculation at the B3LYP/G-31G(d,p) levels. The dove-tailed hydrocarbon chains equipped on the imide unit were replaced by methyl units for simplification, and Fig. S8a (Supporting information) demonstrated the simulated HOMO/LUMO orbital distributions and the calculated energy levels of AnI-SQ and AnI-SeQ. For the LUMO orbitals, both were mainly delocalized throughout the SQ and SeQ skeleton, and the HOMO orbitals were spread over the entire molecular backbones. The HOMO/LUMO energy levels of AnI-SQ and AnI-SeQ were calculated to be −3.32/−6.33 eV and −3.38/−6.21 eV, respectively, and the energy bandgap was 3.01 eV for AnI-SQ and 2.83 eV for AnI-SeQ. Although as-calculated LUMO energy levels were slightly higher than the experimental ones, the regularity of the values is consistent with the experimental data. Besides, from the optimized geometries (Fig. S8c in Supporting information), both AnI-SQ and AnI-SeQ show highly planar conjugated structures, which is beneficial for the close molecular packing.

Furthermore, through the calculated electrostatic potential map (Fig. S8b in Supporting information), the charges distribution of AnI-SQ and AnI-SeQ can be observed. The negative charges (red color) of both AnI-SQ and AnI-SeQ were mainly located at the two oxygen atoms. In contrast, the positive charges (blue color) occupy the other π-conjugated scaffold, especially on the four nitrogen atoms and S/Se atoms in SQ and SeQ, as demonstrated that SQ and SeQ units are more electron-deficient than AnI unit. Additionally, we also calculated and predicted the UV–vis absorption spectra of AnI-SQ and AnI-SeQ (Fig. S10 in Supporting information), AnI-SQ exhibits three major absorption bands with the respective absorption maxima at 230 nm, 327 nm, and 485 nm, and AnI-SeQ also displays three major absorption bands with slight red-shift in contrast to AnI-SQ, showing the absorption maxima of 235 nm, 338 nm, and 495 nm. Such a phenomenon agreed well with our previous experimental data.

Low cytotoxicity of material plays an important role in cell imaging. To investigated the cytotoxic and biocompatibility of AnI-SQ NPs and AnI-SeQ NPs, 3-(4,5-dimethylthiazol-2-yl)−2,5-diphenyl-tetrazolium bromide (MTT) assay was employed to study the biocompatibility without irradiation. 4T1 cells were incubated with different concentrations of AnI-SQ NPs and AnI-SeQ NPs (0, 5, 10, 20, 30, 40 and 50 μg/mL) for 24 h, respectively. As shown in Fig. S9 (Supporting information), the cell viability remained 85% with the treatment of AnI-SeQ NPs and 84% with the treatment of AnI-SQ NPs at a high concentration of 50 μg/mL. As suggests the low cytotoxicity and good biocompatibility of AnI-SQ NPs and AnI-SeQ NPs. The cellular uptake behavior of AnI-SQ NPs in living cells was shown in Fig. 4, AnI-SQ NPs (25 μg/mL) could be well internalized by 4T1 cells. The two-photon fluorescence images of the cells were collected, AnI-SQ NPs were localized in the cytoplasm and showing strong fluorescent at the green channel with excitation at 700 nm, which implied the potentials of AnI-SQ as a two-photon fluorescence imaging agent.

In summary, two polycyclic heteroatom aromatic hydrocarbon molecules AnI-SQ and AnI-SeQ with S and Se-embedment were successfully synthesized, through fusing acenaphthylene-imide and SQ/SeQ together. Upon protonation of the acid-responsive C=N bond, both absorption and emission of AnI-SQ and AnI-SeQ demonstrate an apparent bathochromic shift. The theoretical simulation indicates the highly rigid planar π-conjugated backbones for both AnI-SQ and AnI-SeQ. After self-assembly with Pluronic® F-127, hydrophilic AnI-SeQ nanoparticles (NPs) with low cytotoxicity were applied for the *in vitro* two-photon fluorescence imaging.

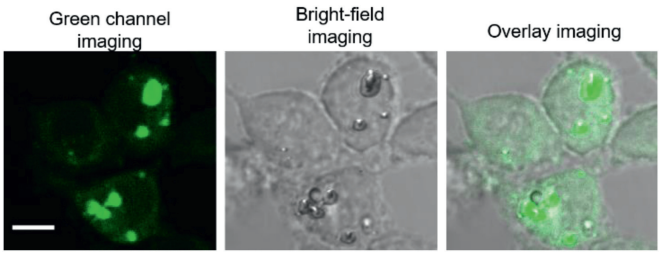

Fig. 4. Two-photon fluorescence imaging of 4T1 cells incubated with 25 μg/mL AnI-SQ NPs at 25 °C. λ_{ex} = 700 nm, scale bar = 10 μm.

Declaration of competing interest

The authors declare that they have no known competing financial interests or personal relationships that could have appeared to influence the work reported in this paper.

Acknowledgments

This work was supported by the Natural Science Foundation of Jiangsu Province (No. BK20200092), and the National Natural Science Foundation of China (No. 21972067). We are also grateful to the High-Performance Computing Center in Nanjing Tech University for supporting the computational resources.

Supplementary materials

Supplementary material associated with this article can be found, in the online version, at doi:10.1016/j.cclet.2021.06.072.

References

[1] X. Cui, C. Xiao, T. Winands, et al., J. Am. Chem. Soc. 140 (2018) 12175–12180.
[2] C. Liu, Y. Ni, X. Lu, G. Li, J. Wu, Acc. Chem. Res. 52 (2019) 2309–2321.
[3] J. Yang, Y. Jiang, Z. Tu, et al., Adv. Funct. Mater. 29 (2019) 1804839.
[4] D. Ji, T. Li, W. Hu, H. Fuchs, Adv. Mater. 31 (2019) 1806070.
[5] Q. Yue, W. Liu, X. Zhu, J. Am. Chem. Soc. 142 (2020) 11613–11628.
[6] M. Stepien, E. Gonka, M. Zyla, N. Sprutta, Chem. Rev. 117 (2017) 3479–3716.
[7] H. Zhang, K. Li, L. Li, Chin. Chem. Lett. 30 (2019) 1063–1066.
[8] B. Zhao, H. Wang, C. Han, et al., Angew. Chem. Int. Ed. 59 (2020) 19042–19047.
[9] J. Yuan, Y. Zhang, L. Zhou, et al., Joule 3 (2019) 1140–1151.
[10] Z. Zhao, C. Chen, W. Wu, et al., Nat. Commun. 10 (2019) 768.
[11] D. Chen, Q. Yu, X. Huang, H. Dai, et al., Small 16 (2020) 2001059.
[12] D. Chen, Z. Wang, H. Dai, et al., Small Methods 4 (2020) 2000013.
[13] F. Xiao, B. Cao, L. Wen, et al., Chin. Chem. Lett. 31 (2020) 2516–2519.
[14] C. Liu, S. Zhang, J. Li, et al., Angew. Chem. Int. Ed. 58 (2019) 1638–1642.
[15] C. Ji, W. Cheng, Q. Yuan, et al., Acc. Chem. Res. 52 (2019) 2266–2277.
[16] H. Dai, Q. Shen, J. Shao, et al., The Innovation 2 (2021) 100082.
[17] B. Joseph, V.K. Sagarika, C. Sabu, et al., J. Bioresour. Bioprod. 5 (2020) 231–247.
[18] H. Xu, D. Zhang, J. Li, J. Bioresour. Bioprod. 4 (2019) 177–182.
[19] Z. Wang, Q. Peng, X. Huang, et al., Dyes Pigm. 185 (2021) 108877.
[20] S. Seifert, D. Schmidt, K. Shoyama, F. Wurthner, Angew. Chem. Int. Ed. 56 (2017) 7595–7600.
[21] Y.J. Hwang, H. Li, B. Courtright, S. Subramaniyan, S.A. Jenekhe, Adv. Mater. 28 (2016) 124–131.
[22] K. Zhou, X. Qiu, L. Xu, et al., ACS Appl. Mater. Interfaces 12 (2020) 14905–14913.
[23] K. Shoyama, M. Mahl, M.A. Niyas, et al., J. Org. Chem. 84 (2019) 142–149.
[24] H. Li, T. Earmme, S. Subramaniyan, S.A. Jenekhe, Adv. Energy Mater. 5 (2015) 1402041.
[25] H. Li, Y.J. Hwang, T. Earmme, et al., Macromolecules 48 (2015) 1759–1766.
[26] H. Li, Y.J. Hwang, B. Courtright, et al., Adv. Mater. 27 (2015) 3266–3272.

[27] J. Shao, X. Guo, N. Shi, et al., Sci. China Mater. 61 (2018) 497–507.
[28] F. Verstraeten, S. Gielen, P. Verstappen, et al., J. Mater. Chem. C 8 (2020) 10098–10103.
[29] C. Costa, J. Farinhas, J. Avó, et al., New J. Chem. 13 (2019) 5202–5213.
[30] S. Li, C. Yin, R. Wang, et al., ACS Appl. Mater. Interfaces 12 (2020) 20281–20286.
[31] X. Du, J. Qi, Z. Zhang, et al., Chem. Mater. 24 (2012) 2178–2185.
[32] F. Liu, S. Wu, Y. Zhang, X. Hao, L. Ding, Sci. Bull. 65 (2020) 698–701.
[33] H. Sun, Y. Tang, C.W. Koh, et al., Adv. Mater. 31 (2019) 1807220.
[34] K. Kise, A. Osuka, Chem. Eur. J. 25 (2019) 15493–15497.
[35] D. Tian, Y. Zhou, Z. Li, et al., ChemistrySelect 2 (2017) 8137–8145.
[36] Z. Cheng, T. Zhang, W. Wang, et al., Chin. Chem. Lett. 32 (2021) 1580–1585.
[37] A.L. Antaris, H. Chen, K. Cheng, et al., Nat. Mater. 14 (2015) 235–242.
[38] L. Xu, H. Zhu, G. Long, et al., J. Mater. Chem. C 3 (2015) 9191–9196.